

An overabundance of low-density Neptune-like planets

Patricio Cubillos^{1*}, Nikolai V. Erkaev², Ines Juvan¹, Luca Fossati¹, Colin P. Johnstone³, Helmut Lammer¹, Monika Lendl¹, Petra Odert¹, and Kristina G. Kislyakova¹

¹ Space Research Institute, Austrian Academy of Sciences, Schmiedlstrasse 6, A-8042 Graz, Austria.

² Federal Research Center "Krasnoyarsk Science Center" SB RAS, "Institute of Computational Modelling".

³ University of Vienna, Department of Astrophysics, Türkenschanzstrasse 17, 1180 Vienna, Austria

Accepted XXX. Received YYY; in original form ZZZ

ABSTRACT

We present a uniform analysis of the atmospheric escape rate of Neptune-like planets with estimated radius and mass (restricted to $M_p < 30 M_\oplus$). For each planet we compute the restricted Jeans escape parameter, Λ , for a hydrogen atom evaluated at the planetary mass, radius, and equilibrium temperature. Values of $\Lambda \lesssim 20$ suggest extremely high mass-loss rates. We identify 27 planets (out of 167) that are simultaneously consistent with hydrogen-dominated atmospheres and are expected to exhibit extreme mass-loss rates. We further estimate the mass-loss rates (L_{hy}) of these planets with tailored atmospheric hydrodynamic models. We compare L_{hy} to the energy-limited (maximum-possible high-energy driven) mass-loss rates. We confirm that 25 planets (15% of the sample) exhibit extremely high mass-loss rates ($L_{\text{hy}} > 0.1 M_\oplus \text{Gyr}^{-1}$), well in excess of the energy-limited mass-loss rates. This constitutes a contradiction, since the hydrogen envelopes cannot be retained given the high mass-loss rates. We hypothesize that these planets are not truly under such high mass-loss rates. Instead, either hydrodynamic models overestimate the mass-loss rates, transit-timing-variation measurements underestimate the planetary masses, optical transit observations overestimate the planetary radii (due to high-altitude clouds), or Neptunes have consistently higher albedos than Jupiter planets. We conclude that at least one of these established estimations/techniques is consistently producing biased values for Neptune planets. Such an important fraction of exoplanets with misinterpreted parameters can significantly bias our view of populations studies, like the observed mass–radius distribution of exoplanets for example.

Key words: planets and satellites: atmospheres – planets and satellites: fundamental parameters – hydrodynamics

1 INTRODUCTION

The Kepler Space Telescope mission has enabled the first estimations of the abundance and size distribution of extrasolar planets in our galaxy (e.g., Fressin et al. 2013; Dressing & Charbonneau 2015). A large fraction of these worlds have sizes intermediate between that of Earth and Neptune, having no analog in our solar system. Further follow-up studies have yielded mass estimates for a large sample of Neptune-like planets (hereafter, considered as those planets with $M_p < 30 M_\oplus \approx 2 M_{\text{Nep}}$), allowing us to study the physical properties of exoplanets in a statistically robust manner.

The planetary radius is inferred from optical transit light-curve observations, typically corresponding to

the $\sim 20 - 100$ mbar level for a clear atmosphere (e.g., Lopez & Fortney 2014; Lammer et al. 2016; Lecavelier des Etangs et al. 2008). The planetary mass, in turn, is inferred either from measurements of the stellar radial velocity (RV) or from transit timing variations (TTV) due to interplanetary perturbations. By combining the mass and radius constraints, we can infer bulk densities and compositions. For a given mass, the planetary radius does not significantly depend on the interior composition, since it is made of very incompressible materials. On the contrary, for a given mass, the hydrogen envelope fraction strongly correlates with the planetary radius (Lopez & Fortney 2014).

The mass–size distribution shows that a considerable fraction of Neptune-like planets have significant envelopes (a few percent of the core mass). Noteworthy, a couple dozen of sub Neptunes show bulk densities far lower than that of the solar-system giant planets. While it is plausi-

* E-mail: patricio.cubillos@oeaw.ac.at

ble that solid cores of a few M_{\oplus} can accrete significant gas envelopes before the protoplanetary disk dissipation (Lee et al. 2014; Inamdar & Schlichting 2015; Stökl et al. 2016; Ginzburg et al. 2016), several studies find that after the disk dispersal these gas envelopes endure significant mass loss due to different mechanisms.

Cooling and photoevaporation, driven by the high-energy stellar irradiation (XUV), produce moderate mass-loss rates and atmospheric contraction. These mechanisms act over timescales larger than $\sim 10^8$ yr (e.g., Lopez et al. 2012; Owen & Wu 2013; Ginzburg et al. 2016). Hydrodynamic and photochemical processes determine the composition of the upper atmosphere of these planets, and therefore of the escaping particles Koskinen et al. (e.g., 2013a,b)

Using hydrodynamic simulations, Owen & Wu (2016) found that during the first \sim Myr after the disk dispersal, low-density planets exhibit extremely high thermally driven mass-loss rates, dubbed “boil-off” (see also Lammer et al. 2016; Fossati et al. 2016). This mechanism consists of hydrodynamic thermal evaporation (Parker wind), driven by the internal heat from the planet, and fueled by the stellar continuum irradiation. During this regime, the atmosphere quickly cools and contracts as it releases energy through the escaped particles. In other words, the thermal energy exceeds the gravitational energy in atmospheric layers where the density is high enough to lead to high mass-loss rates. Consequently, the mass-loss rate exponentially decays until the XUV-driven photoevaporation becomes the dominant mass-loss mechanism (Stökl et al. 2015).

The extremely high mass-loss rates of this regime are unsustainable for the atmospheres of Neptune-like planets over Gyr timescales. Therefore, only young systems are expected to show thermally driven mass-loss rates in excess of the XUV-driven mass-loss rates (Lammer et al. 2016).

Ultraviolet transit observations provide evidence of mass loss on exoplanets (e.g., Vidal-Madjar et al. 2003; Linsky et al. 2010; Fossati et al. 2010; Ben-Jaffel & Ballester 2013). For example, Ly- α transit observations (e.g., Vidal-Madjar et al. 2003; Kulow et al. 2014; Ehrenreich et al. 2015; Bourrier et al. 2016) show transit depths much larger than in the optical. These observations are interpreted as absorption from an extended region of escaping gas beyond the Roche lobe of the planet.

However, the translation from observations into mass-loss rates is very model-dependent. Ly- α observations show large offsets between the absorption features and the center of the line (± 100 km s $^{-1}$), requiring additional assumptions to explain the observations. Among the proposed mechanisms there are: natural broadening from large-scale confinement of material into a higher-density region (Stone & Proga 2009; Owen & Adams 2014), a combination of stellar radiation pressure and wind interactions, where particles accelerate by charge exchange in the wind-wind interaction region (Holmström et al. 2008; Tremblin & Chiang 2013; Kislyakova et al. 2014; Christie et al. 2016), or inhomogeneities of the stellar disc at Ly- α light (Llama et al. 2013).

1.1 Restricted Jeans Escape Parameter

Fossati et al. (2016) described the thermal escape in terms of the classical Jeans escape parameter (see e.g.,

Chamberlain & Hunten 1987). They generalized the Jeans escape parameter for a hydrodynamic atmosphere subjected to the gravitational perturbation from the host star. They studied the upper atmosphere, between the 100 mbar level and the Roche-lobe radius, using hydrodynamic models. By deriving the generalized Jeans escape parameter across the atmospheric layers, they were able to determine how stable a planetary atmosphere is against evaporation.

Fossati et al. (2016) further defined the restricted Jeans escape parameter:

$$\Lambda \equiv \frac{GM_p m_H}{k_B T_{\text{eq}} R_p}, \quad (1)$$

the Jeans escape parameter for a hydrogen atom evaluated at the planetary mass (M_p), radius (R_p), and equilibrium temperature (T_{eq}), where m_H is the mass of the hydrogen atom, G is the gravitational constant, and k_B is the Boltzmann constant. For hydrogen-dominated atmospheres, Λ is an easy-to-calculate parameter that allows one to estimate when the hydrodynamic mass-loss rate exceeds the XUV-driven photoevaporation.

We note that, whereas the classical Jeans escape parameter is a variable as function of altitude in an atmosphere, our definition of Λ is a particular value of it that works as a global parameter for a given planet (no altitude dependence). This is similar to the definition of Guillot et al. (1996), but evaluated at the planetary equilibrium temperature. Using this specific definition, we empirically found the boil-off threshold at $\Lambda \sim 20$ (Fossati et al. 2016), equivalent to the threshold of $R = 0.1 R_{\text{Bondi}}$ of Owen & Wu (2016).

Fossati et al. (2016) determined that planets with $\Lambda \lesssim 20$ –40 should be experiencing extreme mass-loss rates by comparing the hydrodynamic escape rate, L_{hy} , to the maximum XUV-driven escape rate, L_{en} (estimated through the energy-limited formula, Watson et al. 1981), over a range of Λ scenarios with varying stellar type, planetary mass, and planetary radius.

In this paper we follow up the studies of atmospheric escape, modeling and estimating the present-day mass-loss rates for a sample of known exoplanets. We compile a list of the exoplanets with estimated masses and radii, and calculate their restricted Jeans escape parameter, Λ (Section 2). Then, we compute hydrodynamic models tailored for planets suspected of being in the boil-off regime (Section 3). Finally we discuss the observational and physical implications of our findings (Section 4).

2 SAMPLE OF KNOWN NEPTUNES

We compiled our sample by collecting and crosschecking the lists of exoplanets from the Nasa Exoplanet Archive¹ the Exoplanets Data Explorer² (Han et al. 2014), and The Extrasolar Planets Encyclopaedia³ (Schneider et al. 2012). We selected the targets with measured planetary radii and masses, whose mass is less than ~ 2 Neptune masses ($M_p < 30 M_{\oplus}$). We adopted stellar rotational angular velocity (Ω_{rot}) from

¹ <http://exoplanetarchive.ipac.caltech.edu/>

² <http://exoplanets.org/>

³ <http://exoplanet.eu/>

McQuillan et al. (2013) and ages from Morton et al. (2016). Our final sample consists of 167 planets (Table A1).

Fig. 1 shows the mass–radius– T_{eq} distribution for the planets in this sample. We calculated the equilibrium temperature assuming zero Bond albedo and efficient day–night energy redistribution. We split this figure into temperature bins to show representative Λ contours for the planets.

This is a heterogeneous sample of planets. The large majority of these planets (90% of the sample) were discovered using the transit method from the Kepler Space Telescope. The masses of these planets were estimated using the TTV and RV methods (70% and 30% of the sample, respectively), with only a few systems having both TTV and RV constraints: Kepler-18, Kepler-89, K2-19, and WASP-47.

The distribution of planets in Fig. 1 reflects the selection biases from each observing method. Most RV planets fall into the two panels with higher T_{eq} because the RV method favors planets orbiting closer to their host stars. Furthermore, for a given planet size, the RV method tends to find planets with higher mass while the sensitivity of TTVs is more uniform (Weiss & Marcy 2014; Steffen 2016). Jontof-Hutter et al. (2014) argued that larger planets have deeper transits yielding more precise transit times.

Table A1 lists the observed and derived parameters for each planet. We selected the planets consistent with an envelope mass fraction larger than 1% (88 planets) by comparing the observed radii to the models of Lopez & Fortney (2014), for the given planetary masses, stellar ages, and incident fluxes. From this sub sample, we identify 28 planets (17% of the sample) with $\Lambda < 20$, and thus should exhibit extreme mass-loss rates. We note that all of these systems are old (>1 Gyr). We observe some exceptional cases in system parameters, extremely low-bulk-density planets ($\rho_p < 0.2 \text{ g cm}^{-3}$) like Kepler-33, Kepler-51, Kepler-79, Kepler-87, or Kepler-177; and extremely unstable atmospheres ($\Lambda < 5$) like Kepler-33 c or Kepler-51 b.

3 HYDRODYNAMIC RUNS

In this section we present hydrodynamical models of the upper atmosphere of selected Neptune-like planets, which allow us to directly estimate the present-day hydrodynamic mass-loss rate. We further determine whether their mass-loss rate is higher than the upper-limit XUV-driven mass-loss rate. We covered a range of Λ from 0 to 50, including all hydrogen-dominated atmospheres with $\Lambda < 20$, some higher-density planets, and some planets with larger Λ .

To compute L_{hy} , we applied the one-dimensional upper-atmosphere hydrodynamic model of Erkaev et al. (2016). This model solves the hydrodynamic system of equations for mass, momentum, and energy conservation, considering the absorption of stellar XUV flux and accounting for the particles' ionization, dissociation, recombination, and Ly- α cooling⁴.

For the XUV absorption we assume a spherically symmetric distribution of density, deviations from this symmetry do not seem to be essential. One could expect that difference between 1D and 3D models would be more pronounced

for cases of larger Jeans escape parameter, when the hydrodynamic flow is driven mainly by the XUV flux, which may have strong asymmetries. But in such case the mass-loss rate is rather close to the energy-limited escape value, as observed in existing 2D (Khodachenko et al. 2015) and 3D (Tripathi et al. 2015) simulations.

For hot Jupiters, our model produces similar mass-loss rates as most other hydrodynamic models (Erkaev et al. 2016). For the Neptune-like planet GJ 436 b, our model predicts a mass-loss rate of $2 \times 10^{-9} \text{ g s}^{-1}$, consistent with the values from Ehrenreich et al. (2015).

As in Tu et al. (2015) and Johnstone et al. (2015), we calculate the stellar X-ray and EUV luminosities using the scaling laws of Wright et al. (2011) to convert the stellar rotation rates and masses into X-ray luminosities, and Sanz-Forcada et al. (2011) to convert the X-ray luminosities into EUV luminosities. When the stellar rotation rate is not known, we use the gyrochronological relation of Mamajek & Hillenbrand (2008) to convert stellar age into rotation rate.

We calculate the upper-limit XUV-driven escape using the energy-limited formula (Watson et al. 1981; Erkaev et al. 2007):

$$L_{\text{en}} = \frac{\pi \eta R_p (R_{\text{XUV}}^{\text{eff}})^2 F_{\text{XUV}}}{GM_p m_H K}, \quad (2)$$

with $\eta = 15\%$ the net heating efficiency (Shematovich et al. 2014), $R_{\text{XUV}}^{\text{eff}}$ the radius where the bulk of the XUV energy is absorbed, and K the potential energy reduction factor due to stellar tides, which depends on the Roche-lobe boundary radius.

It is important to remark that both the stellar flux and the planetary parameters vary over their respective lifespan, inducing a variation in the planetary mass-loss rate with time (see, e.g., Lecavelier des Etangs et al. 2004; Lecavelier Des Etangs 2007). In particular, for the boil-off regime, Owen & Wu (2016) argue that the mass-loss rate is exponentially sensitive to the planetary radius at small Λ . Thus, during boil-off, strong cooling and contraction quickly reduce R_p (and hence L_{hy}) in timescales of ~ 1 Myr until $\Lambda \sim 20$. The XUV stellar fluxes we compute take into account the age of the star, whereas the planetary radii and masses are taken directly from the reported values. Therefore, the mass-loss rates we compute should be considered as a present-day snapshot of their values.

Table A1 and Fig. 2 show the hydrodynamic and energy-limited mass-loss rates for each modeled planet. Note that the estimated L_{hy} is the total mass-loss rate, including photoevaporation. Thus, we can infer whether photoevaporation ($L_{\text{hy}} \approx L_{\text{en}}$) or boil-off ($L_{\text{hy}} \gg L_{\text{en}}$) is the dominant mass-loss mechanism. Given the variability of L_{hy} and L_{en} with the adopted model parameters (F_{XUV} and η), we consider that planets with $L_{\text{hy}}/L_{\text{en}} > 2.5$ are in the boil-off regime (Lammer et al. 2016).

We confirm that Λ is a good indicator of extreme mass-loss rates (Fig. 2, top panel). For $\Lambda < 15$, $L_{\text{hy}}/L_{\text{en}}$ is strongly correlated with Λ , exponentially increasing with decreasing Λ . In the intermediate range $15 < \Lambda < 25$, there is a transition from boil off to photoevaporation-dominated mass-loss rate. Then, for $\Lambda > 25$, $L_{\text{hy}}/L_{\text{en}}$ remains constant as the mass-loss rate is dominated by the XUV-driven photoevaporation. We find no significant correlation of Λ with

⁴ See the appendix in Erkaev et al. (2016) for a detailed description.

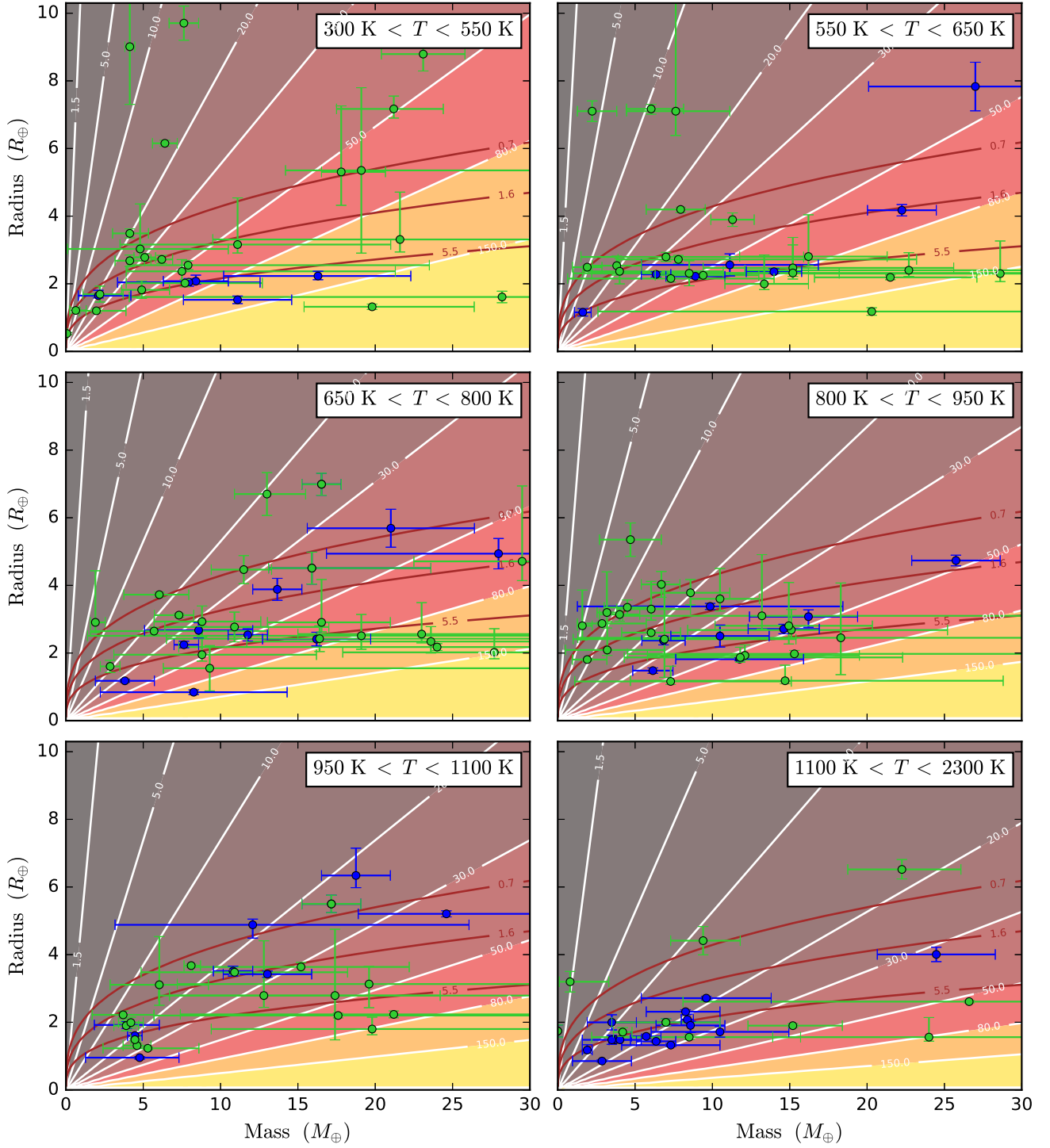


Figure 1. Mass–radius– T_{eq} distribution of the known Neptune-like planets. The blue and green markers denote RV- and TTV-measured masses, respectively. From top to bottom, the brown solid lines denote constant-density curves corresponding to Saturn’s, Neptune’s, and Earth’s bulk density in g cm^{-3} , respectively. The background color contour denotes the value of Λ for the mean equilibrium temperature of the planets in each panel: 455, 600, 715, 870, 1025, and 1440 K. Note that the Λ -contours work only as a guideline, Table A1 gives the specific values for each planet.

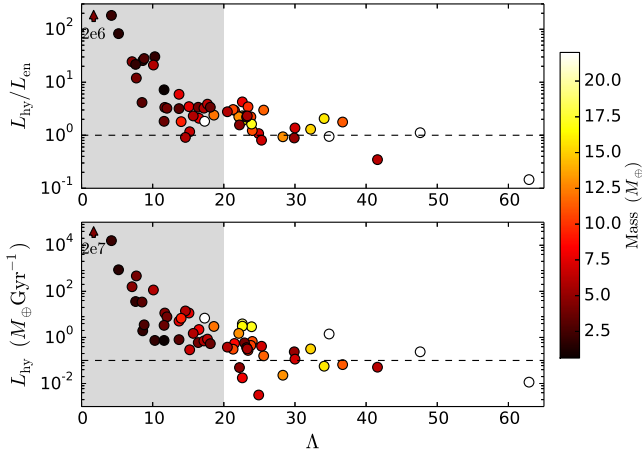


Figure 2. Top: Ratio between the hydrodynamic and energy-limited mass-loss rate *vs.* Λ . The color scale denotes the planetary mass. The background color marks the regions with dominant thermal mass-loss rate (gray) and XUV-driven photoevaporation (white). The labeled triangle denotes the mass-loss values for the extreme case of Kepler-33 c. Bottom: Hydrodynamic mass-loss rate *vs.* Λ .

other observed parameters. Furthermore, 19 of the 27 previously identified planets with hydrogen-dominated atmospheres and $\Lambda < 20$ satisfy $L_{\text{hy}}/L_{\text{en}} > 2.5$. Six additional low-density planets with $\Lambda \leq 25$ also present an excess mass-loss rate. The bottom panel of Fig. 2 shows the computed hydrodynamic mass-loss rates. All planets with excess mass-loss rates ($L_{\text{hy}}/L_{\text{en}} > 2.5$) show hydrodynamic mass-loss rates above $0.1 M_{\oplus} \text{Gyr}^{-1}$. At this rate, these planets should have already lost their hydrogen atmospheres.

The scatter in L_{hy} (Fig. 2, bottom panel) seems to be mainly correlated with the planetary mass: at a given Λ more massive planets have higher mass-loss rates. On the contrary, the main source for the scatter in $L_{\text{hy}}/L_{\text{en}}$ (Fig. 2, top panel) is unclear; these variations seem to be a more complex combination of several factors, e.g., Roche-lobe radius, incident stellar flux, XUV absorption radius, etc.

4 DISCUSSION

The observed low bulk densities of many Neptune-like planets require a significant hydrogen envelope fraction. However, their estimated restricted Jeans escape parameter, Λ , and further hydrodynamic modeling indicate that 25 planets in our sample (15%) should be experiencing extremely high mass-loss rates ($L_{\text{hy}} > 0.1 M_{\oplus} \text{Gyr}^{-1}$) in excess of the maximum XUV-driven photoevaporation ($L_{\text{hy}}/L_{\text{en}} > 2.5$).

Considering the age of the systems (\gtrsim Gyr), it is improbable that these Neptunes have retained their hydrogen envelopes until the present day. In addition, the short timescale of the boil-off regime (\lesssim Myr) makes it unlikely that we are observing a transient phenomenon by chance. This contradiction leads us to consider biases on the mass-loss model estimations, the measured physical parameters, or the physical interpretation of the observations.

4.1 Hydrodynamic-model Bias?

Validating model mass-loss rates is challenging because to date there are no direct observational measurements. UV transit observations depend as much on the hydrodynamic models inside the planetary Roche lobe as in the particle dynamics after. This would require a treatment of a number of physical processes that are largely unconstrained (e.g., magnetic fields, stellar radiation pressure, wind-wind interaction).

The heating efficiency rate η is one of the least constrained parameters in our model, for which we assume a value of 0.15. A detailed calculation of η is complicated, as it varies with altitude and it requires a kinetic approach considering many chemical reactions. Shematovich et al. (2014) estimated values of η between 0.1 and 0.2 for hot Jupiters. Assuming larger heating efficiency one can increase the mass-loss rates; however, Owen & Jackson (2012) discarded values larger than $\eta = 0.4$. Salz et al. (2016) found little variation of the heating efficiency ($\eta \approx 0.1\text{--}0.3$) with gravitational potential, except for the most compact and massive planets.

One process that we do not consider is magnetic fields. Owen & Adams (2014) and Khodachenko et al. (2015) found that magnetic fields can suppress mass-loss rates by approximately an order of magnitude by confining the outflowing material into smaller opening angles around the poles.

4.2 Planetary-mass Bias?

One explanation to this contradiction is that TTV analyses are underestimating the planetary masses, a possibility already considered by Weiss & Marcy (2014). A more massive planet would have a stronger gravitational pull, decreasing the mass-loss rate. Steffen (2016) argues that the mass measurements derived from RV and TTV are comparably reliable since the physics behind TTV measurements (gravity) is well understood. However, given the complexity and rapid-pace development of exoplanet RV and TTV analyses, as data-reduction techniques improve, their mass estimations continuously get overturned or refined. For example, TTV-estimated masses for Kepler-114 c (Xie 2014), Kepler-231 c (Kipping et al. 2014), and Kepler-56 b (Huber et al. 2013) differ by a factor of ten from a nearly contemporaneous estimation (Hadden & Lithwick 2014). Cases of extremely high densities (e.g., Kepler-327 c, $\rho_p \approx 70 \text{ g cm}^{-3}$ Hadden & Lithwick 2014) or even negative RV-estimated masses (e.g., Marcy et al. 2014) serve as reminders to use the data-reduction and statistical tools with caution. One should incorporate all available prior information (e.g., in a Bayesian posterior sampling) to avoid results at odds with physical principles.

In our sample, with the exception of Kepler-94 b, all boil-off planets have TTV-determined masses. Ideally, comparing the TTV and RV results for a given system would test the reliability of these techniques. However, due to the observing limitations of each method, only a couple of systems have allowed for independent TTV and RV analyses. For example, for the Kepler-89 system, Masuda et al. (2013) found discrepancies between the TTV and RV-mass estimations. On the contrary, for the Kepler-18 and WASP-

47 systems, TTV and RV analyses return consistent results (Cochran et al. 2011; Dai et al. 2015).

If we adopted masses such that $\Lambda \equiv 20$ (M_{20} , keeping all other parameters fixed), 13 of the 19 low-density extreme-mass-loss planets with $\Lambda < 20.0$ would have a mass correction larger than $1\sigma_M$, with a mean of $5.0\sigma_M$ (see Table 1).

4.3 Planetary-radius Bias?

Another possibility is that we are misinterpreting the observed transit radius. For clear atmospheres in Neptune-like planets, the observed optical transit radius corresponds to the ~ 20 – 100 mbar level (Lopez & Fortney 2014; Lammer et al. 2016). However, if a planet has high-altitude, optically thick clouds/hazes, the transit radius would be overestimating the planetary radius. If this is the case, then the true 100 mbar altitude would correspond to a smaller radius than the observed radius, yielding moderate mass-loss rates. Spectroscopic analyses already indicate that many Neptune and sub-Neptune sized planets show flat transmission spectra, consistent with gray opacity hazes or clouds (e.g., Kreidberg et al. 2014; Knutson et al. 2014; Ehrenreich et al. 2014).

If we adopted radii such that $\Lambda \equiv 20$ (R_{20} , keeping all other parameters fixed), 18 of the 19 low-density boil-off planets with $\Lambda < 20.0$ would have a radius correction larger than $1\sigma_R$, with a mean of $8.5\sigma_R$ (see Table 1). Adopting R_{20} as the 100 mbar pressure level, we computed hydrostatic-equilibrium pressure–radius profiles to calculate the observed transit photospheric pressure, $p_{\text{phot}} = p(R_p)$. Table 1 shows that a third of the planets could have photospheres at pressures between 10^{-3} bar and 10^{-7} bar, compatible with the location of cloud decks on exoplanets.

When we plot the planetary surface gravity, $\log g$, vs. equilibrium temperature for the planets in our sample (Fig. 3, top panel), we see that all boil-off planets are grouped in the $\log g < 3.0$ region. While it is not surprising that these planets are concentrated at low $\log g$ values (given the similarity in mass and radius dependency of $\log g \propto M_p R_p^{-2}$ and $\Lambda \propto M_p R_p^{-1}$), it is interesting that this region limits closely to the boundary between strong and weak J-band H₂O features observed in hot Jupiters, associated to cloudy vs. clear atmospheres, respectively (Stevenson 2016). Regardless of whether there is a link between cloud processes on hot Jupiters and Neptune-like planets—two completely different samples—, this graph helps to identify planets with a higher prominence of clouds/hazes. Note that the derived surface gravity of these planets is also affected by the observational biases. Fig. 3 (bottom panel) shows the corrected $\log g$ – T_{eq} position of the boil-off planets if we assumed R_{20} as the 100 mbar radius.

An important remark to highlight is that, while our analysis suggests that boil-off planets can have instead moderate mass-loss rates if they have cloudy atmospheres, we cannot claim that the remaining planets have clear atmospheres. They can either host clear or cloudy atmospheres. This occurs because our analysis is based on the dominant effect of hydrogen in the observed planetary radius. There can be cloudy planets with secondary atmospheres, or even hydrogen-dominated atmospheres hosting lower-

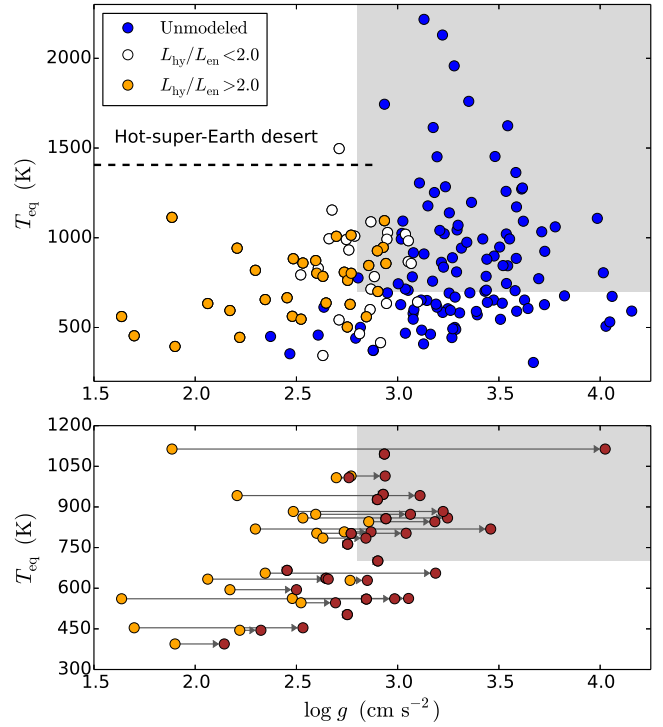


Figure 3. Planetary surface gravity vs. equilibrium-temperature. The orange, white, and blue circles (top panel) denote the extreme mass-loss rate, moderate mass-loss rate, and unmodeled planets, respectively. The gray and white background colors denote the region where planets have clear and cloudy-atmospheres, respectively, derived by Stevenson (2016) for hot Jupiters. The horizontal dashed line denotes the lowest incident-stellar-flux boundary ($650 F_{\oplus}$) of the hot-super-Earth desert (Lundkvist et al. 2016). The bottom panel shows the expected $\log g$ of the boil-off planets if their radii were corrected to have $\Lambda \equiv 20.0$ (brown circles) relative to their initial position (orange circles).

altitude clouds that do not alter much the observed transit radius.

4.4 Bond-albedo Bias?

The cloudy-atmospheres scenario has a second consequence on the properties of these planets. The high-altitude cloud/haze layer would reflect a larger fraction of the incident stellar irradiation, decreasing the amount of energy deposited in the atmosphere, and consequently decreasing the estimated mass-loss rates. Low-density sub Neptunes (on average) would then differ from hot Jupiters. Studies of the aggregate sample of hot Jupiters show low geometric optical albedos ($A_g \approx 0.1$) and somewhat higher Bond albedos ($A_B = 0.4 \pm 0.1$, Schwartz & Cowan 2015), suggesting that hot Jupiters have a layer of optical absorbers above an infrared reflective cloud deck. Our cloudy-atmosphere case aligns well with the higher geometric albedos ($A_g \approx 0.16 - 0.3$) found on super-Earth planets ($R_p < 2.5R_{\oplus}$, Demory 2014).

Table 1 shows the required values of the Bond albedo such that $\Lambda \equiv 20.0$ (A_{20} , keeping all other parameters fixed). Most of the planets in this list would require Bond albedos higher than any observed value from solar or extrasolar gaseous planet.

If we confirm the cloudy nature of these atmo-

Table 1. Low-density boil-off planet parameters. Λ , M_p , R_p , and T_{eq} are as in Table A1. M_{20} , R_{20} , and A_{20} are the modified mass, radius, and bond albedo such that $\Lambda = 20$. p_{phot} is the photospheric pressure corresponding to R_p when we adopt R_{20} as the 100 mbar pressure level.

Planet name	Λ	M_p M_{\oplus}	M_{20} M_{\oplus}	R_p R_{\oplus}	R_{20} R_{\oplus}	p_{phot} bar	T_{eq} K	A_{20}
Kepler-11 c	8.8	$2.86^{+2.86}_{-1.59}$	6.5	$2.87^{+0.04}_{-0.06}$	1.26	6.8×10^{-13}	859	0.96
Kepler-11 f	10.3	1.91 ± 0.95	3.7	$2.49^{+0.04}_{-0.07}$	1.29	2.4×10^{-11}	562	0.93
Kepler-114 d	18.1	3.81 ± 1.59	4.2	2.54 ± 0.28	2.30	1.4×10^{-03}	628	0.32
Kepler-177 b	7.6	$1.91^{+0.64}_{-0.32}$	5.0	$2.91^{+1.53}_{-0.30}$	1.10	4.7×10^{-14}	655	0.98
Kepler-177 c	13.7	$7.63^{+3.50}_{-3.18}$	11.1	$7.10^{+3.71}_{-0.72}$	4.87	5.5×10^{-08}	594	0.78
Kepler-254 c	13.7	$3.20^{+3.70}_{-2.70}$	4.7	$2.09^{+0.84}_{-0.16}$	1.44	5.5×10^{-08}	845	0.78
Kepler-29 b	11.7	4.50 ± 1.50	7.7	3.35 ± 0.22	1.95	5.0×10^{-10}	872	0.88
Kepler-29 c	12.0	4.00 ± 1.30	6.6	3.14 ± 0.20	1.89	1.2×10^{-09}	802	0.87
Kepler-305 c	17.2	$6.04^{+2.54}_{-2.22}$	7.0	$3.30^{+0.82}_{-0.33}$	2.83	1.4×10^{-04}	808	0.46
Kepler-307 b	8.5	3.18 ± 0.64	7.4	$3.20^{+1.20}_{-0.46}$	1.36	4.1×10^{-13}	883	0.97
Kepler-307 c	5.2	$1.59^{+0.64}_{-0.32}$	6.1	$2.81^{+1.05}_{-0.42}$	0.74	2.3×10^{-16}	818	0.99
Kepler-33 c	1.7	$0.80^{+2.50}_{-0.70}$	9.4	3.20 ± 0.30	0.27	6.7×10^{-20}	1113	0.99
Kepler-33 d	7.1	4.70 ± 2.00	13.3	5.35 ± 0.49	1.89	1.3×10^{-14}	941	0.98
Kepler-51 b	4.2	$2.22^{+1.59}_{-0.95}$	10.5	7.10 ± 0.30	1.50	2.3×10^{-17}	561	0.99
Kepler-51 c	7.7	4.13 ± 0.32	10.8	$9.01^{+2.81}_{-1.71}$	3.45	5.3×10^{-14}	453	0.98
Kepler-51 d	15.1	7.63 ± 0.95	10.1	9.71 ± 0.50	7.34	1.3×10^{-06}	394	0.67
Kepler-79 d	10.1	$6.04^{+2.10}_{-1.59}$	12.0	$7.17^{+0.13}_{-0.16}$	3.61	1.4×10^{-11}	633	0.94
Kepler-79 e	16.4	$4.13^{+1.21}_{-1.11}$	5.0	3.49 ± 0.13	2.87	2.7×10^{-05}	546	0.54
Kepler-87 c	17.7	6.40 ± 0.80	7.2	6.15 ± 0.09	5.46	5.1×10^{-04}	444	0.38

spheres, this analysis places strong constraints on the atmospheric properties of the ensemble of low-density sub Neptunes. These planets would present high-altitude opaque clouds/hazes that increase the observed radii. Observationally, the value of their restricted Jeans escape parameter Λ , and also their position in the $\log g - T_{\text{eq}}$ plane, would be simple and direct indicators of the cloud/haze prominence on the atmospheres of these planets.

On a different but still interesting topic, the distribution of planets in the $\log g - T_{\text{eq}}$ plane (Fig. 3 top panel) agrees well with the proposed hot-super-Earth desert (Lundkvist et al. 2016). The boundary at 650 times the incident flux on Earth (F_{\oplus}) directly translates into an equilibrium temperature of ~ 1400 K. From the planets with known mass and radius, we observe a dearth of planets above this line. Unlike the $R_p - F_{\oplus}$ figure from Lundkvist et al. (2016), this figure further constrains the parameter space of the planetary physical properties of the desert by adding information from the masses (through the surface gravity).

Furthermore, by considering the boil-off mass-loss regime, our results (Fig. 3 bottom panel) suggest that the exoplanet desert extends even further. Be it the mass or the radius of the planets being misinterpreted, boil-off planets should have a higher surface gravity, further depleting a region below the $T_{\text{eq}} = 1400$ K boundary, down to ~ 600 K.

5 CONCLUSIONS

We studied the mass-loss rates of the sample of 167 confirmed planets with masses $M_p < 30M_{\oplus}$. For 15% of the planets in this sample, we found that their planetary

mass, radius, and equilibrium temperature lead to paradoxical results. Their observed low bulk densities imply hydrogen-dominated atmospheres. However, hydrodynamical models indicate extremely high mass-loss rates ($L_{\text{hy}} > 0.1 M_{\oplus} \text{Gyr}^{-1}$), thus being unable to retain their hydrogen envelopes (boil-off regime).

Our hydrodynamical models' mass-loss rates agree well with state-of-the-art models from the literature. Unfortunately, current observations do not offer a direct, model-independent validation of escape rates. Magnetic fields (however largely unknown) could offer a solution of this paradox by decreasing the predicted mass-loss rates (Owen & Adams 2014; Khodachenko et al. 2015). Alternatively, the boil-off timescales of $\sim 10^6$ yr (Owen & Wu 2016) could have been grossly underestimated. We need more detailed studies of the mass-loss time evolution during the boil-off regime.

If the model mass-loss estimations are correct, we hypothesize that either the TTV studies are underestimating the planetary masses or that these planets have high-altitude clouds/hazes producing overestimated transit radii, high albedos, or both. The cloudy/hazy scenario is further supported by the higher albedo found for super Earths, and a similar correlation as that between $\log g - T_{\text{eq}}$ and clear/cloudy atmospheres for hot Jupiters.

Whether we are misinterpreting their observed transit radii or underestimating their TTV masses, a fraction of ~ 10 – 20% Neptunes with biased parameters will have a large impact on the population studies of the mass-radius relationship. Both empirical laws and physically motivated models tracing the observed mass-radius distribution of Neptunes would be disrupted by this sub-sample, simply because the observed values are not representative of the underlying

properties of exoplanets. This could explain, for example, why studies like [Wolfgang & Lopez \(2015\)](#) do not find a direct mass–radius relationship for sub Neptune planets. In the future, population studies should consider the added complexity introduced by this rather large sub-sample of planets.

Conclusively solving this puzzle involves a multitude of studies, from the confirmation of low-densities with RV measurements, to the consistent modeling of high-altitude clouds/hazes. This study generates many open questions for the future, for example, can clouds/hazes form and remain at such high altitudes and under strong stellar irradiation conditions? Or how do reflective clouds affect the atmospheric albedo, and hence mass loss?

ACKNOWLEDGMENTS

We thank contributors to SciPy, Matplotlib ([Hunter 2007](#)), the Python Programming Language, and contributors to the free and open-source community. We thank the anonymous referee for comments that significantly improved the quality of the paper. This research has made use of the Exoplanet Orbit Database and the Exoplanet Data Explorer at [exoplanets.org](#) and the NASA Exoplanet Archive, which is operated by the California Institute of Technology, under contract with the National Aeronautics and Space Administration under the Exoplanet Exploration Program. We acknowledge the Austrian Forschungsförderungsgesellschaft FFG projects “RASEN” P847963 and “TAPAS4CHEOPS” P853993, the Austrian Science Fund (FWF) NFN projects S11607-N16 and S11604-N16, and the FWF project P27256-N27. N.V.E. acknowledges support by the RFBR grant No. 15-05-00879-a and No. 16-52-14006 ANF-a.

REFERENCES

- Almenara J. M., et al., 2015, *A&A*, **581**, L7
 Alonso R., et al., 2014, *A&A*, **567**, A112
 Bakos G. Á., et al., 2010, *ApJ*, **710**, 1724
 Barros S. C. C., et al., 2014, *A&A*, **569**, A74
 Barros S. C. C., et al., 2015, *MNRAS*, **454**, 4267
 Becker J. C., Vanderburg A., Adams F. C., Rappaport S. A., Schwengeler H. M., 2015, *ApJ*, **812**, L18
 Ben-Jaffel L., Ballester G. E., 2013, *A&A*, **553**, A52
 Berta-Thompson Z. K., et al., 2015, *Nature*, **527**, 204
 Biddle L. I., et al., 2014, *MNRAS*, **443**, 1810
 Borucki W. J., et al., 2010, *ApJ*, **713**, L126
 Bourrier V., Lecavelier des Etangs A., Ehrenreich D., Tanaka Y. A., Vidotto A. A., 2016, *A&A*, **591**, A121
 Carter J. A., et al., 2012, *Science*, **337**, 556
 Chamberlain J. W., Hunten D. M., 1987, Theory of planetary atmospheres. An introduction to their physics and chemistry.
 Christie D., Arras P., Li Z.-Y., 2016, *ApJ*, **820**, 3
 Cochran W. D., et al., 2011, *ApJS*, **197**, 7
 Dai F., et al., 2015, *ApJ*, **813**, L9
 Demory B.-O., 2014, *ApJ*, **789**, L20
 Demory B.-O., et al., 2011, *A&A*, **533**, A114
 Dressing C. D., Charbonneau D., 2015, *ApJ*, **807**, 45
 Dressing C. D., et al., 2015, *ApJ*, **800**, 135
 Ehrenreich D., et al., 2014, *A&A*, **570**, A89
 Ehrenreich D., et al., 2015, *Nature*, **522**, 459
 Erkaev N. V., Kulikov Y. N., Lammer H., Selsis F., Langmayr D., Jaritz G. F., Biernat H. K., 2007, *A&A*, **472**, 329
 Erkaev N. V., Lammer H., Odert P., Kislyakova K. G., Johnstone C. P., Güdel M., Khodachenko M. L., 2016, *MNRAS*, **460**, 1300
 Espinoza N., et al., 2016, *ApJ*, **830**, 43
 Fossati L., et al., 2010, *ApJ*, **714**, L222
 Fossati L., Erkaev N. V., Lammer H., Cubillos P., Juvan I., Kislyakova K. G., Lendl M., Odert P., 2016, *A&A*, Submitted.
 Fressin F., et al., 2013, *ApJ*, **766**, 81
 Gautier III T. N., et al., 2012, *ApJ*, **749**, 15
 Gettel S., et al., 2016, *ApJ*, **816**, 95
 Gilliland R. L., et al., 2013, *ApJ*, **766**, 40
 Ginzburg S., Schlichting H. E., Sari R., 2016, *ApJ*, **825**, 29
 Guillot T., Burrows A., Hubbard W. B., Lunine J. I., Saumon D., 1996, *ApJ*, **459**, L35
 Hadden S., Lithwick Y., 2014, *ApJ*, **787**, 80
 Hadden S., Lithwick Y., 2016, *ApJ*, **828**, 44
 Han E., Wang S. X., Wright J. T., Feng Y. K., Zhao M., Fakhouri O., Brown J. I., Hancock C., 2014, *PASP*, **126**, 827
 Harpsøe K. B. W., et al., 2013, *A&A*, **549**, A10
 Hartman J. D., et al., 2011, *ApJ*, **728**, 138
 Holmström M., Ekenbäck A., Selsis F., Penz T., Lammer H., Wurz P., 2008, *Nature*, **451**, 970
 Huber D., et al., 2013, *Science*, **342**, 331
 Hunter J. D., 2007, Computing In Science & Engineering, 9, 90
 Inamdar N. K., Schlichting H. E., 2015, *MNRAS*, **448**, 1751
 Johnstone C. P., et al., 2015, *ApJ*, **815**, L12
 Jontof-Hutter D., Lissauer J. J., Rowe J. F., Fabrycky D. C., 2014, *ApJ*, **785**, 15
 Jontof-Hutter D., Rowe J. F., Lissauer J. J., Fabrycky D. C., Ford E. B., 2015, *Nature*, **522**, 321
 Jontof-Hutter D., et al., 2016, *ApJ*, **820**, 39
 Khodachenko M. L., Shaikhislamov I. F., Lammer H., Prokopov P. A., 2015, *ApJ*, **813**, 50
 Kipping D. M., Nesvorný D., Buchhave L. A., Hartman J., Bakos G. Á., Schmitt A. R., 2014, *ApJ*, **784**, 28
 Kislyakova K. G., Holmström M., Lammer H., Odert P., Khodachenko M. L., 2014, *Science*, **346**, 981
 Knutson H. A., Benneke B., Deming D., Homeier D., 2014, *Nature*, **505**, 66
 Koskinen T. T., Harris M. J., Yelle R. V., Lavvas P., 2013a, *Icarus*, **226**, 1678
 Koskinen T. T., Yelle R. V., Harris M. J., Lavvas P., 2013b, *Icarus*, **226**, 1695
 Kreidberg L., et al., 2014, *Nature*, **505**, 69
 Kulow J. R., France K., Linsky J., Loyd R. O. P., 2014, *ApJ*, **786**, 132
 Lammer H., et al., 2016, preprint, ([arXiv:1605.03595](#))
 Lecavelier Des Etangs A., 2007, *A&A*, **461**, 1185
 Lecavelier des Etangs A., Vidal-Madjar A., McConnell J. C., Hébrard G., 2004, *A&A*, **418**, L1
 Lecavelier des Etangs A., Pont F., Vidal-Madjar A., Sing D., 2008, *A&A*, **481**, L83
 Lee E. J., Chiang E., Ormel C. W., 2014, *ApJ*, **797**, 95
 Linsky J. L., Yang H., France K., Froning C. S., Green J. C., Stocke J. T., Osterman S. N., 2010, *ApJ*, **717**, 1291
 Lissauer J. J., et al., 2013, *ApJ*, **770**, 131
 Llama J., Vidotto A. A., Jardine M., Wood K., Fares R., Gombosi T. I., 2013, *MNRAS*, **436**, 2179
 Lopez E. D., Fortney J. J., 2014, *ApJ*, **792**, 1
 Lopez E. D., Fortney J. J., Miller N., 2012, *ApJ*, **761**, 59
 Lundkvist M. S., et al., 2016, *Nature Communications*, **7**, 11201
 Maciejewski G., Niedzielski A., Nowak G., Pallé E., Tingley B., Errmann R., Neuhäuser R., 2014, *Acta Astronomica*, **64**, 323
 Mamajek E. E., Hillenbrand L. A., 2008, *ApJ*, **687**, 1264
 Marcy G. W., et al., 2014, *ApJS*, **210**, 20
 Masuda K., 2014, *ApJ*, **783**, 53
 Masuda K., Hirano T., Taruya A., Nagasawa M., Suto Y., 2013, *ApJ*, **778**, 185

- McQuillan A., Mazeh T., Aigrain S., 2013, *ApJ*, **775**, L11
- Morton T. D., Bryson S. T., Coughlin J. L., Rowe J. F., Ravichandran G., Petigura E. A., Haas M. R., Batalha N. M., 2016, *ApJ*, **822**, 86
- Motalebi F., et al., 2015, *A&A*, **584**, A72
- Moutou C., et al., 2014, *MNRAS*, **444**, 2783
- Nesvorný D., Kipping D., Terrell D., Hartman J., Bakos G. Á., Buchhave L. A., 2013, *ApJ*, **777**, 3
- Ofir A., Dreizler S., Zechmeister M., Husser T.-O., 2014, *A&A*, **561**, A103
- Owen J. E., Adams F. C., 2014, *MNRAS*, **444**, 3761
- Owen J. E., Jackson A. P., 2012, *MNRAS*, **425**, 2931
- Owen J. E., Wu Y., 2013, *ApJ*, **775**, 105
- Owen J. E., Wu Y., 2016, *ApJ*, **817**, 107
- Pepe F., et al., 2013, *Nature*, **503**, 377
- Petigura E. A., et al., 2016, *ApJ*, **818**, 36
- Salz M., Schneider P. C., Czesla S., Schmitt J. H. M. M., 2016, *A&A*, **585**, L2
- Sanchis-Ojeda R., et al., 2012, *Nature*, **487**, 449
- Sanz-Forcada J., Micela G., Ribas I., Pollock A. M. T., Eiroa C., Velasco A., Solano E., García-Álvarez D., 2011, *A&A*, **532**, A6
- Schmitt J. R., et al., 2014, *ApJ*, **795**, 167
- Schneider J., Le Sidaner P., Savalle R., Zolotukhin I., 2012, in Ballester P., Egret D., Lorente N. P. F., eds, *Astronomical Society of the Pacific Conference Series Vol. 461, Astronomical Data Analysis Software and Systems XXI*. p. 447
- Schwartz J. C., Cowan N. B., 2015, *MNRAS*, **449**, 4192
- Shematovich V. I., Ionov D. E., Lammer H., 2014, *A&A*, **571**, A94
- Steffen J. H., 2016, *MNRAS*, **457**, 4384
- Stevenson K. B., 2016, *ApJ*, **817**, L16
- Stökl A., Dorfi E., Lammer H., 2015, *A&A*, **576**, A87
- Stökl A., Dorfi E. A., Johnstone C. P., Lammer H., 2016, *ApJ*, **825**, 86
- Stone J. M., Proga D., 2009, *ApJ*, **694**, 205
- Tremblin P., Chiang E., 2013, *MNRAS*, **428**, 2565
- Tripathi A., Kratter K. M., Murray-Clay R. A., Krumholz M. R., 2015, *ApJ*, **808**, 173
- Tu L., Johnstone C. P., Güdel M., Lammer H., 2015, *A&A*, **577**, L3
- Van Grootel V., et al., 2014, *ApJ*, **786**, 2
- Vanderburg A., et al., 2015, *ApJ*, **800**, 59
- Vidal-Madjar A., Lecavelier des Etangs A., Désert J.-M., Ballester G. E., Ferlet R., Hébrard G., Mayor M., 2003, *Nature*, **422**, 143
- Watson A. J., Donahue T. M., Walker J. C. G., 1981, *Icarus*, **48**, 150
- Weiss L. M., Marcy G. W., 2014, *ApJ*, **783**, L6
- Weiss L. M., et al., 2013, *ApJ*, **768**, 14
- Weiss L. M., et al., 2016, *ApJ*, **819**, 83
- Wolfgang A., Lopez E., 2015, *ApJ*, **806**, 183
- Wright N. J., Drake J. J., Mamajek E. E., Henry G. W., 2011, *ApJ*, **743**, 48
- Xie J.-W., 2013, *ApJS*, **208**, 22
- Xie J.-W., 2014, *ApJS*, **210**, 25

APPENDIX A: PARAMETERS OF THE KNOWN NEPTUNE PLANETS

Table A1 list the observed and derived parameters for the known sample of Neptune-like planets.

This paper has been typeset from a $\text{\TeX}/\text{\LaTeX}$ file prepared by the author.

Table A1. Observed and derived parameters for the sub-Neptune planet sample. This table only includes planets with estimated mass (M_p) and transit radius (R_p), with $M_p < 30M_\oplus$. The equilibrium temperature (T_{eq}) assumes zero Bond albedo and efficient day–night energy redistribution. The restricted Jeans escape parameter (Λ) comes from Eq. (1). The planetary mean density (ρ_p) assumes the observed mass and transit radius. F_{XUV} (section 3) is the stellar XUV-flux received by the planet for the given orbital semi-major axis (a), stellar mass (M_s), age, and rotational angular velocity (Ω_{rot}). L_{hy} and L_{en} (section 3) are the hydrodynamic and energy-limited XUV-driven (L_{en}) mass-loss rates of the selected hydrodynamic-modeled planets (mostly low-density planets with $\Lambda < 20$).

Name	M_p M_\oplus	R_p R_\oplus	T_{eq} K	Λ	ρ_p g cm^{-3}	a AU	M_s M_\odot	Age Gyr	Ω_{rot} Ω_\odot	F_{XUV} $\text{erg s}^{-1} \text{cm}^{-2}$	L_{hy} s^{-1}	L_{en} s^{-1}	$L_{\text{hy}}/L_{\text{en}}$	Ref. ^{a,b}
55 Cnc e	8.38±0.39	2.08±0.16	1957	15.6	5.14	0.015	0.91	10.2	1.4	173333.5	De11 ^R
CoRoT-22 b	12.08 ^{+13.99} _{-8.90}	4.88 ^{+0.17} _{-0.39}	1007	18.6	0.57	0.092	1.10	3.3	1.9	10959.0	3.4×10 ³⁵	1.4×10 ³⁵	2.3	Mou14 ^R
CoRoT-24 c	27.97±11.12	4.94±0.45	706	60.8	1.28	0.098	0.91	11.0	1.3	2429.9	Alo14 ^R
CoRoT-7 b	5.72±0.95	1.58±0.07	1760	15.6	7.97	0.017	0.91	1.3	2.3	293392.3	Ba14 ^R
EPIC 2037 b	21.01±5.40	5.69±0.56	776	36.1	0.63	0.154	1.12	5.0	0.4	231.6	Pet15 ^R
EPIC 2037 c	27.00±6.90	7.83±0.72	612	42.7	0.31	0.247	1.12	5.0	0.4	90.0	Pet15 ^R
GJ 1132 b	1.62±0.54	1.16±0.11	578	18.4	5.79	0.015	0.18	5.0	5.2	156736.6	BT15 ^R
GJ 1214 b	6.36±0.95	2.28±0.08	599	35.3	2.97	0.014	0.18	6.0	5.2	181777.4	Ha13 ^R
GJ 3470 b	13.67±1.59	3.88±0.33	692	38.5	1.29	0.031	0.51	2.5	...	5353.9	Bi14 ^R
GJ 436 b	22.25±2.22	4.17±0.17	642	62.9	1.69	0.029	0.47	6.0	0.3	699.6	1.3×10 ³³	8.9×10 ³³	0.1	Mac14 ^R
HAT-P-11 b	25.75±2.86	4.74±0.16	866	47.6	1.34	0.053	0.81	6.5	1.1	5944.9	2.7×10 ³⁴	2.4×10 ³⁴	1.1	Bak10 ^R
HAT-P-26 b	18.75±2.22	6.34 ^{+0.81} _{-0.36}	994	22.6	0.41	0.048	0.82	9.0	1.2	12237.8	4.4×10 ³⁵	2.4×10 ³⁵	1.8	Ha11 ^R
HD 219134 b	4.46±0.47	1.61±0.09	1022	20.6	5.94	0.038	0.79	12.5	0.3	926.6	Mot15 ^R
HD 97658 b	7.63 ^{+0.95} _{-0.64}	2.24 ^{+0.10} _{-0.09}	758	34.0	3.72	0.080	0.77	6.0	0.4	485.1	VG14 ^R
HIP 116454 b	11.76±1.27	2.54±0.18	691	50.8	3.98	0.091	0.78	2.0	1.5	4879.7	V15 ^R
K2-19 c	15.90 ^{+7.70} _{-2.80}	4.51±0.47	783	34.1	0.96	0.100	0.95	...	0.5	540.3	6.4×10 ³³	3.2×10 ³³	2.0	Ba15 ^{R,T}
K2-3 b	8.40±2.10	2.08 ^{+0.18} _{-0.09}	500	61.3	5.18	0.077	0.61	2.0	...	1232.2	Alm15 ^R
K2-3 c	2.10 ^{+2.10} _{-1.30}	1.65 ^{+0.16} _{-0.07}	371	26.0	2.58	0.141	0.61	2.0	...	374.9	Alm15 ^R
K2-3 d	11.10±3.50	1.53±0.11	305	180.8	17.22	0.209	0.61	2.0	...	170.1	Alm15 ^R
K2-56 b	16.30 ^{+6.00} _{-6.10}	2.23 ^{+0.14} _{-0.11}	545	101.6	8.11	0.241	0.96	3.3	1.9	1517.7	E16 ^R
Kepler-10 b	3.72±0.42	1.48 ^{+0.04} _{-0.03}	2129	8.9	6.31	0.017	0.91	9.1	1.0	124224.8	W16 ^R
Kepler-10 c	13.98±1.79	2.36 ^{+0.09} _{-0.04}	570	78.8	5.89	0.240	0.91	9.1	1.0	639.6	W16 ^R
Kepler-100 b	7.31±3.18	1.32±0.04	1271	32.9	17.37	0.073	1.08	6.9	1.3	14282.2	Mar14 ^R
Kepler-102 d	3.81±1.91	1.18±0.04	701	35.0	12.86	0.086	0.81	4.1	0.4	302.8	Mar14 ^R
Kepler-102 e	8.90±1.91	2.22±0.07	604	50.3	4.47	0.117	0.81	4.1	0.4	166.5	Mar14 ^R
Kepler-103 b	9.85±8.58	3.38±0.09	946	23.4	1.41	0.128	1.09	6.0	0.9	2165.8	3.1×10 ³⁴	9.0×10 ³³	3.4	Mar14 ^R
Kepler-104 b	19.60 ^{+14.50} _{-12.40}	3.13 ^{+0.52} _{-0.70}	1043	45.5	3.53	0.094	0.81	3.7	...	5720.3	HL14 ^T
Kepler-105 b	3.70±2.00	2.22±0.11	1088	11.6	1.87	0.060	0.96	3.5	1.6	17615.2	3.8×10 ³⁵	2.1×10 ³⁵	1.8	JH15b ^T
Kepler-105 c	4.60±0.90	1.31±0.07	993	26.8	11.28	0.072	0.96	3.5	1.6	12198.6	JH15b ^T
Kepler-106 c	10.49±3.18	2.50±0.33	863	36.8	3.69	0.111	1.00	3.3	0.2	68.5	Mar14 ^R
Kepler-106 e	11.12±5.72	2.56±0.33	583	56.5	3.66	0.243	1.00	3.3	0.2	14.3	Mar14 ^R
Kepler-11 b	1.91 ^{+1.27} _{-0.95}	1.81 ^{+0.03} _{-0.04}	931	8.6	1.78	0.091	0.96	6.9	0.2	175.8	2.2×10 ³⁵	8.7×10 ³³	25.3	L13 ^T
Kepler-11 c	2.86 ^{+2.86} _{-1.59}	2.87 ^{+0.04} _{-0.06}	859	8.8	0.67	0.107	0.96	6.9	0.2	127.2	4.0×10 ³⁵	1.5×10 ³⁴	26.7	L13 ^T
Kepler-11 d	7.31 ^{+0.95} _{-1.59}	3.12 ^{+0.06} _{-0.07}	714	24.9	1.33	0.155	0.96	6.9	0.2	60.6	3.6×10 ³²	3.5×10 ³²	1.0	L13 ^T
Kepler-11 e	7.95 ^{+1.59} _{-2.22}	4.20 ^{+0.07} _{-0.09}	636	22.6	0.59	0.195	0.96	6.9	0.2	38.3	2.0×10 ³³	4.9×10 ³²	4.1	L13 ^T
Kepler-11 f	1.91±0.95	2.49 ^{+0.04} _{-0.07}	562	10.3	0.68	0.250	0.96	6.9	0.2	23.3	8.4×10 ³⁴	2.8×10 ³³	30.0	L13 ^T
Kepler-113 b	11.76±4.13	1.82±0.04	844	58.1	10.80	0.050	0.75	3.2	0.3	635.2	Mar14 ^R
Kepler-114 c	2.86±0.64	1.60±0.18	714	18.9	3.82	0.065	0.56	2.7	0.9	4657.9	X14 ^T
Kepler-114 d	3.81±1.59	2.54±0.28	628	18.1	1.29	0.083	0.56	2.7	0.9	2796.6	6.1×10 ³⁴	1.8×10 ³⁴	3.4	X14 ^T
Kepler-120 b	8.50 ^{+9.70} _{-7.50}	2.31±0.37	613	45.5	3.80	0.055	0.59	3.6	...	1524.5	HL14 ^T
Kepler-122 e	27.70 ^{+11.40} _{-9.80}	2.02 ^{+0.70} _{-0.19}	676	153.8	18.53	0.227	0.99	3.9	...	1104.9	HL14 ^T
Kepler-131 b	16.21±3.50	2.41±0.20	785	64.9	6.37	0.126	1.02	3.7	0.2	79.2	Mar14 ^R
Kepler-131 c	8.26±6.04	0.84±0.07	673	110.6	76.46	0.171	1.02	3.7	0.2	42.9	Mar14 ^R
Kepler-136 b	19.80 ^{+11.70} _{-10.40}	1.80 ^{+0.35} _{-0.17}	1060	78.6	18.72	0.106	1.20	2.8	...	12210.7	HL14 ^T
Kepler-138 b	0.07 ^{+0.06} _{-0.04}	0.53±0.03	449	2.1	2.51	0.075	0.52	4.7	1.4	2705.8	JH15a ^T
Kepler-138 c	1.97 ^{+1.91} _{-1.12}	1.20±0.07	408	30.5	6.28	0.090	0.52	4.7	1.4	1838.5	JH15a ^T
Kepler-138 d	0.64 ^{+0.67} _{-0.39}	1.21±0.08	343	11.6	1.98	0.128	0.52	4.7	1.4	924.8	8.4×10 ³⁴	1.2×10 ³⁴	7.1	JH15a ^T

Table A1 – continued Sub-Neptune Planet Parameters.

Name	M_p M_\oplus	R_p R_\oplus	T_{eq} K	Λ	ρ_p $g\ cm^{-3}$	a AU	M_s M_\odot	Age Gyr	Ω_{rot} Ω_\odot	F_{XUV} $erg\ s^{-1}\ cm^{-2}$	L_{hy} s^{-1}	L_{en} s^{-1}	L_{hy}/L_{en}	Ref. ^{a,b}
Kepler-161 b	12.10 ^{+7.40} _{-6.30}	1.93 ^{+0.31} _{-0.14}	948	50.1	9.28	0.054	0.77	4.7	1.0	7681.3	HL14 ^T
Kepler-161 c	11.80 ^{+10.50} _{-7.50}	1.87 ^{+0.30} _{-0.14}	844	56.6	9.95	0.068	0.77	4.7	1.0	4844.0	HL14 ^T
Kepler-176 c	23.00 ^{+13.50} _{-8.00}	2.56 ^{+0.93} _{-0.26}	745	91.4	7.56	0.102	0.83	4.7	0.8	1567.5	HL14 ^T
Kepler-176 d	15.20 ^{+10.40} _{-5.80}	2.47 ^{+0.90} _{-0.25}	589	79.2	5.56	0.163	0.83	4.7	0.8	613.8	HL14 ^T
Kepler-177 b	1.91 ^{+0.64} _{-0.32}	2.91 ^{+1.53} _{-0.30}	655	7.6	0.43	0.222	1.07	4.4	...	962.8	4.1×10 ³⁶	2.0×10 ³⁵	20.5	X14 ^T
Kepler-177 c	7.63 ^{+3.50} _{-3.18}	7.10 ^{+3.71} _{-0.72}	594	13.7	0.12	0.270	1.07	4.4	...	651.5	5.8×10 ³⁵	1.0×10 ³⁵	5.8	X14 ^T
Kepler-18 b	6.99±3.50	2.00±0.10	1284	20.7	4.84	0.045	0.97	10.7	1.9	46258.8	Co11 ^{R,T}
Kepler-18 c	17.16±1.91	5.50±0.26	990	23.9	0.57	0.075	0.97	10.7	1.9	16344.6	3.3×10 ³⁵	2.1×10 ³⁵	1.6	Co11 ^{R,T}
Kepler-18 d	16.53±1.27	6.99±0.33	793	22.6	0.27	0.117	0.97	10.7	1.9	6729.1	3.5×10 ³⁵	1.9×10 ³⁵	1.8	Co11 ^{R,T}
Kepler-184 c	8.80 ^{+7.40} _{-5.70}	1.95 ^{+0.84} _{-0.19}	693	49.4	6.55	0.141	0.87	4.5	...	1017.7	HL14 ^T
Kepler-189 c	22.70 ^{+17.10} _{-10.60}	2.40 ^{+0.52} _{-0.18}	590	121.5	9.06	0.137	0.84	5.2	...	497.7	HL14 ^T
Kepler-197 c	5.30 ^{+3.30} _{-2.90}	1.23±0.04	1021	32.0	15.71	0.090	0.92	5.4	...	3777.0	HL14 ^T
Kepler-20 b	8.58±2.22	1.91 ^{+0.12} _{-0.21}	1197	28.5	6.82	0.045	0.91	5.2	0.2	732.8	Ga12 ^R
Kepler-20 c	16.21 ^{+3.18} _{-3.81}	3.07 ^{+0.20} _{-0.31}	836	47.8	3.08	0.093	0.91	5.2	0.2	174.6	Ga12 ^R
Kepler-211 c	18.30 ^{+22.40} _{-17.00}	2.45 ^{+1.62} _{-1.09}	898	63.1	6.86	0.062	0.97	1.6	2.0	12588.9	HL14 ^T
Kepler-215 d	23.60 ^{+17.30} _{-11.90}	2.34 ^{+0.44} _{-0.34}	652	117.1	10.16	0.185	0.77	1.6	...	2352.6	HL14 ^T
Kepler-219 d	19.10 ^{+29.90} _{-17.70}	2.51 ^{+0.63} _{-0.40}	652	88.4	6.66	0.272	1.15	4.6	1.6	1158.9	HL14 ^T
Kepler-221 c	15.10 ^{+10.10} _{-6.70}	2.68 ^{+0.61} _{-0.26}	942	45.3	4.33	0.059	0.72	4.6	2.9	70313.6	HL14 ^T
Kepler-226 b	24.00 ^{+11.80} _{-10.10}	1.56 ^{+0.58} _{-0.12}	1108	105.3	34.86	0.047	0.86	4.4	...	7076.1	HL14 ^T
Kepler-23 b	15.20 ^{+3.20} _{-2.90}	1.90±0.06	1277	47.5	12.22	0.075	1.11	6.6	...	8385.5	HL14 ^T
Kepler-23 d	17.60 ^{+13.70} _{-11.90}	2.20±0.07	993	61.1	9.12	0.124	1.11	6.6	...	3067.7	HL14 ^T
Kepler-231 b	4.90 ^{+1.80} _{-1.30}	1.82 ^{+0.26} _{-0.25}	462	44.1	4.48	0.074	0.51	3.5	1.2	2185.7	K14 ^T
Kepler-231 c	2.20 ^{+1.50} _{-1.10}	1.69 ^{+0.24} _{-0.23}	372	26.5	2.51	0.114	0.51	3.5	1.2	921.0	K14 ^T
Kepler-238 f	13.35 ^{+2.86} _{-2.54}	2.00 ^{+0.85} _{-0.17}	635	79.8	9.24	0.272	1.06	6.8	...	507.0	X14 ^T
Kepler-244 d	15.20 ^{+20.00} _{-13.00}	2.32 ^{+0.83} _{-0.18}	640	77.6	6.71	0.140	0.88	4.8	...	720.1	HL14 ^T
Kepler-245 d	21.60 ^{+16.60} _{-12.10}	3.31 ^{+1.40} _{-0.37}	489	101.1	3.28	0.202	0.80	3.6	1.4	987.3	HL14 ^T
Kepler-25 b	9.60±4.20	2.71±0.05	1305	20.6	2.65	0.070	1.19	2.9	3.9	92614.7	Mar14 ^R
Kepler-25 c	24.60±5.70	5.21±0.09	1029	34.8	0.96	0.113	1.19	2.9	3.9	35845.4	1.6×10 ³⁵	1.7×10 ³⁵	0.9	Mar14 ^R
Kepler-254 c	3.20 ^{+3.70} _{-2.70}	2.09 ^{+0.84} _{-0.16}	845	13.7	1.93	0.105	0.97	4.0	1.1	2984.8	9.1×10 ³⁴	2.9×10 ³⁴	3.1	HL14 ^T
Kepler-26 b	5.10±0.70	2.78±0.11	465	29.9	1.31	0.085	0.54	3.0	2.0	5260.6	2.7×10 ³⁴	2.8×10 ³⁴	1.0	JH15b ^T
Kepler-26 c	6.20±0.70	2.72±0.12	415	41.6	1.70	0.107	0.54	3.0	2.0	3338.5	5.8×10 ³³	1.7×10 ³⁴	0.3	JH15b ^T
Kepler-27 c	21.20 ^{+3.20} _{-3.70}	7.17 ^{+0.38} _{-0.27}	457	49.0	0.32	0.191	0.65	1.6	0.5	222.8	HL14 ^T
Kepler-276 c	16.53 ^{+4.45} _{-3.50}	2.91 ^{+1.27} _{-0.28}	669	64.4	3.71	0.203	1.10	3.8	...	1237.2	X14 ^T
Kepler-276 d	16.21 ^{+5.09} _{-4.45}	2.81 ^{+1.23} _{-0.27}	581	75.4	4.05	0.269	1.10	3.8	...	704.2	X14 ^T
Kepler-28 b	8.80 ^{+3.80} _{-3.10}	2.93±0.46	743	30.6	1.93	0.062	0.75	2.2	1.5	7830.8	HL14 ^T
Kepler-28 c	10.90 ^{+6.10} _{-4.50}	2.77±0.44	650	45.9	2.83	0.081	0.75	2.2	1.5	4587.9	HL14 ^T
Kepler-289 b	7.31±6.67	2.15±0.10	630	40.8	4.03	0.210	1.08	3.8	3.0	4490.4	S14 ^T
Kepler-289 d	4.13±0.95	2.68±0.17	502	23.2	1.18	0.330	1.08	3.8	3.0	1818.4	4.1×10 ³⁴	1.9×10 ³⁴	2.2	S14 ^T
Kepler-29 b	4.50±1.50	3.35±0.22	872	11.7	0.66	0.092	0.98	...	2.3	13666.1	1.3×10 ³⁶	4.0×10 ³⁵	3.3	JH15b ^T
Kepler-29 c	4.00±1.30	3.14±0.20	802	12.0	0.71	0.109	0.98	...	2.3	9778.1	8.9×10 ³⁵	2.8×10 ³⁵	3.2	JH15b ^T
Kepler-30 b	11.30±1.40	3.90±0.20	599	36.7	1.05	0.186	0.99	1.6	1.1	718.8	7.5×10 ³³	4.3×10 ³³	1.7	SO12 ^T
Kepler-30 d	23.10±2.70	8.79±0.50	353	56.4	0.19	0.534	0.99	1.6	1.1	86.7	SO12 ^T
Kepler-305 b	10.49 ^{+2.54} _{-1.91}	3.60 ^{+0.90} _{-0.36}	927	23.8	1.24	0.056	0.76	4.4	...	3742.0	5.1×10 ³⁴	2.4×10 ³⁴	2.1	X14 ^T
Kepler-305 c	6.04 ^{+2.54} _{-2.22}	3.30 ^{+0.82} _{-0.33}	808	17.2	0.93	0.073	0.76	4.4	...	2158.9	8.0×10 ³⁴	2.5×10 ³⁴	3.2	X14 ^T
Kepler-307 b	3.18±0.64	3.20 ^{+1.20} _{-0.46}	883	8.5	0.54	0.093	0.98	6.6	2.0	11054.6	3.9×10 ³⁶	9.5×10 ³⁵	4.1	X14 ^T
Kepler-307 c	1.59 ^{+0.64} _{-0.32}	2.81 ^{+1.05} _{-0.42}	818	5.2	0.40	0.108	0.98	6.6	2.0	8159.4	9.8×10 ³⁷	1.2×10 ³⁶	81.7	X14 ^T
Kepler-31 c	29.50 ^{+9.60} _{-7.00}	4.71 ^{+2.23} _{-0.57}	653	72.7	1.56	0.260	1.21	4.2	...	1108.1	HL14 ^T
Kepler-32 b	9.40 ^{+3.60} _{-3.10}	2.25±0.11	595	53.2	4.55	0.050	0.54	2.7	0.8	2232.3	HL14 ^T
Kepler-32 c	7.70 ^{+5.00} _{-3.80}	2.02±0.11	443	65.1	5.15	0.090	0.54	2.7	0.8	689.0	HL14 ^T
Kepler-326 c	17.40 ^{+15.40} _{-10.70}	2.79 ^{+1.96} _{-1.31}	974	48.5	4.42	0.051	0.98	4.7	2.8	34240.8	HL14 ^T
Kepler-326 d	6.90 ^{+8.50} _{-5.90}	2.41 ^{+1.70} _{-1.13}	856	25.3	2.72	0.066	0.98	4.7	2.8	20445.5	4.7×10 ³⁴	6.1×10 ³⁴	0.8	HL14 ^T

Table A1 – *continued* Sub-Neptune Planet Parameters.

Name	M_p M_\oplus	R_p R_\oplus	T_{eq} K	Λ	ρ_p g cm^{-3}	a AU	M_s M_\odot	Age Gyr	Ω_{rot} Ω_\odot	F_{XUV} $\text{erg s}^{-1} \text{cm}^{-2}$	L_{hy} s^{-1}	L_{en} s^{-1}	$L_{\text{hy}}/L_{\text{en}}$	Ref. ^{a,b}
Kepler-327 c	20.30 ^{+27.10} _{-17.70}	1.18±0.11	591	220.6	68.14	0.047	0.55	3.0	1.1	4264.3	HL14 ^T
Kepler-328 b	28.61 ^{+13.03} _{-12.40}	2.30 ^{+0.97} _{-0.24}	627	150.3	12.96	0.219	1.15	2.6	...	1487.0	X14 ^T
Kepler-33 c	0.80 ^{+2.50} _{-0.70}	3.20±0.30	1113	1.7	0.13	0.119	1.29	4.4	1.0	2707.6	2.2×10 ⁴²	1.4×10 ³⁶	1.6×10 ⁶	HL16 ^T
Kepler-33 d	4.70±2.00	5.35±0.49	941	7.1	0.17	0.166	1.29	4.4	1.0	1385.8	1.8×10 ³⁷	7.5×10 ³⁵	24.0	HL16 ^T
Kepler-33 e	6.70 ^{+1.20} _{-1.30}	4.03±0.38	830	15.2	0.57	0.214	1.29	4.4	1.0	837.4	3.3×10 ³⁴	2.8×10 ³⁴	1.2	HL16 ^T
Kepler-33 f	11.50 ^{+1.80} _{-2.10}	4.47±0.42	762	25.6	0.71	0.254	1.29	4.4	1.0	595.6	1.8×10 ³⁴	6.1×10 ³³	3.0	HL16 ^T
Kepler-333 b	28.20 ^{+29.00} _{-24.10}	1.61±0.17	506	262.1	37.27	0.087	0.54	3.2	1.1	2381.1	HL14 ^T
Kepler-338 e	8.50 ^{+7.20} _{-6.30}	1.56±0.07	1258	32.8	12.35	0.090	1.10	4.8	...	10799.4	HL14 ^T
Kepler-339 c	7.30 ^{+7.80} _{-6.20}	1.16 ^{+0.45} _{-0.09}	924	51.6	25.79	0.069	0.84	4.4	1.6	13691.2	HL14 ^T
Kepler-339 d	14.70 ^{+14.10} _{-10.00}	1.18 ^{+0.46} _{-0.09}	804	117.4	49.34	0.091	0.84	4.4	1.6	7871.5	HL14 ^T
Kepler-350 c	6.04±3.18	3.11 ^{+1.43} _{-0.61}	1009	14.6	1.11	0.134	1.00	3.2	8.5	243252.4	1.6×10 ³⁶	1.8×10 ³⁶	0.9	X14 ^T
Kepler-350 d	14.94 ^{+5.40} _{-4.77}	2.81 ^{+1.28} _{-0.54}	888	45.4	3.73	0.172	1.00	3.2	8.5	146470.2	X14 ^T
Kepler-351 b	4.80 ^{+5.70} _{-4.70}	3.03 ^{+1.33} _{-0.24}	542	22.2	0.95	0.214	0.89	4.9	...	356.0	5.6×10 ³³	3.6×10 ³³	1.6	HL14 ^T
Kepler-351 c	11.10 ^{+9.90} _{-7.60}	3.16 ^{+1.38} _{-0.25}	468	56.9	1.94	0.287	0.89	4.9	...	197.9	HL14 ^T
Kepler-36 b	4.46 ^{+0.33} _{-0.27}	1.48±0.03	1069	21.3	7.52	0.115	1.07	4.8	1.6	10334.7	Ca12 ^T
Kepler-36 c	8.10 ^{+0.60} _{-0.46}	3.68±0.05	1014	16.5	0.90	0.128	1.07	4.8	1.6	8348.0	2.5×10 ³⁵	1.2×10 ³⁵	2.1	Ca12 ^T
Kepler-385 b	12.80 ^{+11.40} _{-6.80}	2.79 ^{+1.62} _{-0.35}	1041	33.4	3.25	0.097	1.09	3.3	...	8110.4	HL14 ^T
Kepler-385 c	13.20 ^{+16.80} _{-9.00}	3.10 ^{+1.81} _{-0.39}	909	35.5	2.44	0.127	1.09	3.3	...	4731.3	HL14 ^T
Kepler-396 c	17.80 ^{+2.86} _{-1.27}	5.31 ^{+1.95} _{-0.99}	440	57.7	0.66	0.368	0.85	4.4	2.0	1032.9	X14 ^T
Kepler-4 b	24.47±3.81	4.01±0.21	1614	28.7	2.10	0.046	1.22	6.8	0.8	9535.9	Bo10 ^R
Kepler-406 b	6.36±1.27	1.44±0.03	1452	23.1	11.83	0.036	1.07	2.1	0.2	758.8	Mar14 ^R
Kepler-406 c	2.86±1.91	0.85±0.03	1171	21.7	25.43	0.056	1.07	2.1	0.2	321.0	Mar14 ^R
Kepler-454 b	6.84±1.40	2.37±0.13	916	23.9	2.83	0.095	1.03	4.3	1.2	4051.6	Ge15 ^R
Kepler-48 b	3.94±2.10	1.92±0.10	1024	15.2	3.07	0.053	0.88	6.2	0.3	759.5	Mar14 ^R
Kepler-48 c	14.61±2.30	2.71±0.14	809	50.5	4.05	0.085	0.88	6.2	0.3	296.8	Mar14 ^R
Kepler-48 d	7.95±4.61	2.04±0.11	492	59.9	5.14	0.230	0.88	6.2	0.3	40.7	Mar14 ^R
Kepler-49 b	7.80 ^{+15.40} _{-3.90}	2.72±0.12	627	34.7	2.14	0.060	0.55	2.9	1.5	8833.6	X13 ^T
Kepler-49 c	7.90 ^{+15.60} _{-3.90}	2.55±0.13	546	43.0	2.63	0.079	0.55	2.9	1.5	5074.4	X13 ^T
Kepler-51 b	2.22 ^{+1.59} _{-0.95}	7.10±0.30	561	4.2	0.03	0.251	1.04	3.4	3.3	3724.8	1.8×10 ³⁹	1.0×10 ³⁷	180.0	Mas14 ^T
Kepler-51 c	4.13±0.32	9.01 ^{+2.81} _{-1.71}	453	7.7	0.03	0.384	1.04	3.4	3.3	1596.5	5.3×10 ³⁷	4.5×10 ³⁶	11.8	Mas14 ^T
Kepler-51 d	7.63±0.95	9.71±0.50	394	15.1	0.05	0.509	1.04	3.4	3.3	908.7	1.3×10 ³⁶	3.8×10 ³⁵	3.4	Mas14 ^T
Kepler-54 b	21.50 ^{+5.60} _{-4.90}	2.19±0.07	605	122.9	11.29	0.063	0.51	4.2	0.8	2727.7	HL14 ^T
Kepler-54 c	19.80 ^{+6.60} _{-4.40}	1.32±0.08	530	214.3	47.48	0.082	0.51	4.2	0.8	1610.1	HL14 ^T
Kepler-56 b	22.25 ^{+3.81} _{-3.50}	6.52 ^{+0.29} _{-0.28}	1496	17.3	0.44	0.103	1.32	4.4	...	18720.8	7.8×10 ³⁵	4.2×10 ³⁵	1.9	H13 ^T
Kepler-57 c	9.30 ^{+25.20} _{-3.00}	1.55±0.67	705	64.5	13.77	0.092	0.76	4.7	0.8	1761.3	X13 ^T
Kepler-60 b	4.20±0.60	1.71±0.13	1177	15.8	4.63	0.073	1.04	5.1	...	8080.2	JH15b ^T
Kepler-60 c	3.90±0.80	1.90±0.15	1092	14.2	3.14	0.085	1.04	5.1	...	5999.3	JH15b ^T
Kepler-60 d	4.20±0.80	1.99±0.16	992	16.1	2.94	0.103	1.04	5.1	...	4082.8	JH15b ^T
Kepler-65 c	26.60 ^{+20.40} _{-18.50}	2.61±0.04	1363	56.7	8.25	0.068	1.25	3.3	4.0	96951.2	HL14 ^T
Kepler-68 b	8.26 ^{+2.22} _{-2.54}	2.31 ^{+0.06} _{-0.09}	1252	21.7	3.69	0.062	1.08	6.3	0.2	441.3	Gi13 ^R
Kepler-68 c	4.77 ^{+2.54} _{-3.50}	0.95 ^{+0.03} _{-0.04}	1033	36.7	30.30	0.091	1.08	6.3	0.2	204.7	Gi13 ^R
Kepler-78 b	1.91±0.32	1.18 ^{+0.16} _{-0.09}	2217	5.5	6.43	0.009	0.76	0.8	1.7	731021.4	Pep13 ^R
Kepler-79 b	10.90 ^{+7.31} _{-6.04}	3.48±0.07	992	24.0	1.43	0.117	1.17	3.2	...	6920.5	7.6×10 ³⁴	6.3×10 ³⁴	1.2	JH14 ^T
Kepler-79 c	6.04 ^{+1.91} _{-2.29}	3.73±0.08	784	15.7	0.64	0.187	1.17	3.2	...	2709.1	1.7×10 ³⁵	7.4×10 ³⁴	2.3	JH14 ^T
Kepler-79 d	6.04 ^{+2.10} _{-1.59}	7.17 ^{+0.13} _{-0.16}	633	10.1	0.09	0.287	1.17	3.2	...	1150.1	1.3×10 ³⁷	6.1×10 ³⁵	21.3	JH14 ^T
Kepler-79 e	4.13 ^{+1.21} _{-1.11}	3.49±0.13	546	16.4	0.54	0.386	1.17	3.2	...	635.8	6.8×10 ³⁴	2.0×10 ³⁴	3.4	JH14 ^T
Kepler-80 b	5.70 ^{+7.40} _{-5.50}	2.65±0.11	700	23.3	1.69	0.065	0.72	2.9	1.1	3568.7	3.6×10 ³⁴	1.6×10 ³⁴	2.3	X13 ^T
Kepler-80 c	7.00 ^{+8.90} _{-5.50}	2.79±0.13	633	30.0	1.77	0.079	0.72	2.9	1.1	2391.0	1.3×10 ³⁴	9.6×10 ³³	1.4	X13 ^T
Kepler-81 b	16.40 ^{+27.00} _{-9.90}	2.42±0.38	707	72.5	6.35	0.055	0.64	3.6	2.0	17772.7	X13 ^T
Kepler-81 c	4.00 ^{+6.70} _{-2.40}	2.37±0.37	559	22.9	1.66	0.089	0.64	3.6	2.0	6948.7	6.6×10 ³⁴	3.0×10 ³⁴	2.2	X13 ^T
Kepler-82 c	19.10 ^{+55.50} _{-4.90}	5.35±2.45	500	54.0	0.69	0.257	0.85	4.7	...	265.2	X13 ^T

Table A1 – *continued* Sub-Neptune Planet Parameters.

Name	M_p M_\oplus	R_p R_\oplus	T_{eq} K	Λ	ρ_p g cm^{-3}	a AU	M_s M_\odot	Age Gyr	Ω_{rot} Ω_\odot	F_{XUV} $\text{erg s}^{-1} \text{cm}^{-2}$	L_{hy} s^{-1}	L_{en} s^{-1}	$L_{\text{hy}}/L_{\text{en}}$	Ref. ^{a,b}
Kepler-83 c	$7.50^{+13.80}_{-3.60}$	2.37 ± 0.35	485	49.5	3.12	0.126	0.66	3.1	1.8	2880.2	X13 ^T
Kepler-84 b	$21.20^{+32.00}_{-13.80}$	2.23 ± 0.10	1092	65.9	10.50	0.083	1.00	9.6	1.4	11252.1	X13 ^T
Kepler-85 b	$15.30^{+22.10}_{-10.80}$	1.97 ± 0.10	884	66.4	10.95	0.078	0.92	4.0	1.2	4726.9	X13 ^T
Kepler-85 c	$24.00^{+34.40}_{-16.70}$	2.18 ± 0.10	771	108.3	12.83	0.103	0.92	4.0	1.2	2738.9	X13 ^T
Kepler-87 c	6.40 ± 0.80	6.15 ± 0.09	444	17.7	0.15	0.671	1.10	7.2	1.3	178.9	9.6×10^{34}	2.5×10^{34}	3.8	O14 ^T
Kepler-88 b	8.58 ± 2.54	$3.78^{+0.39}_{-0.36}$	801	21.5	0.88	0.095	0.96	2.2	1.1	2566.9	6.2×10^{34}	2.2×10^{34}	2.8	N13 ^T
Kepler-89 b	10.49 ± 4.45	1.72 ± 0.16	1624	28.5	11.43	0.051	1.28	3.3	2.6	78217.2	W13 ^R
Kepler-89 c	$9.40^{+2.40}_{-2.10}$	4.41 ± 0.42	1154	14.0	0.60	0.101	1.28	3.3	2.6	20126.4	7.7×10^{35}	4.3×10^{35}	1.8	Mas13 ^T
Kepler-89 e	$13.00^{+2.50}_{-2.10}$	6.70 ± 0.63	665	22.1	0.24	0.305	1.28	3.3	2.6	2227.5	1.7×10^{35}	7.7×10^{34}	2.2	Mas13 ^T
Kepler-92 c	6.04 ± 1.91	2.60 ± 0.08	856	20.5	1.89	0.186	1.21	5.9	1.7	3067.7	4.3×10^{34}	1.6×10^{34}	2.8	X14 ^T
Kepler-93 b	4.02 ± 0.68	1.48 ± 0.02	1138	18.1	6.82	0.053	0.91	5.2	0.3	942.4	Dr15 ^R
Kepler-94 b	10.81 ± 1.27	3.51 ± 0.15	1095	21.3	1.38	0.034	0.81	2.5	0.4	1815.1	3.5×10^{34}	1.2×10^{34}	2.9	Mar14 ^R
Kepler-95 b	13.03 ± 2.86	3.42 ± 0.09	1019	28.3	1.79	0.102	1.08	8.7	0.3	281.0	2.6×10^{33}	2.8×10^{33}	0.9	Mar14 ^R
Kepler-96 b	8.58 ± 3.50	2.67 ± 0.22	782	31.2	2.48	0.125	1.00	3.7	0.3	128.8	Mar14 ^R
Kepler-97 b	3.50 ± 1.91	1.48 ± 0.13	1451	12.3	5.93	0.036	0.94	4.6	0.3	1966.4	Mar14 ^R
Kepler-98 b	3.50 ± 1.59	2.00 ± 0.22	1743	7.6	2.42	0.026	0.99	8.3	0.2	2774.0	Mar14 ^R
Kepler-99 b	6.15 ± 1.30	1.48 ± 0.08	880	35.8	10.46	0.050	0.79	4.3	0.4	883.3	Mar14 ^R
WASP-47 d	15.20 ± 7.00	3.64 ± 0.13	983	32.2	1.74	0.086	1.04	...	1.4	6812.1	3.6×10^{34}	2.8×10^{34}	1.3	Be15 ^T

^a References for Planetary Masses and Radii. Alm15: [Almenara et al. \(2015\)](#), Alo14: [Alonso et al. \(2014\)](#), BT15: [Berta-Thompson et al. \(2015\)](#), Ba14: [Barros et al. \(2014\)](#), Ba15: [Barros et al. \(2015\)](#), Bak10: [Bakos et al. \(2010\)](#), Be15: [Becker et al. \(2015\)](#), Bi14: [Biddle et al. \(2014\)](#), Bo10: [Borucki et al. \(2010\)](#), Ca12: [Carter et al. \(2012\)](#), Co11: [Cochran et al. \(2011\)](#), De11: [Demory et al. \(2011\)](#), Dr15: [Dressing et al. \(2015\)](#), E16: [Espinoza et al. \(2016\)](#), Ga12: [Gautier et al. \(2012\)](#), Ge15: [Gettel et al. \(2016\)](#), Gi13: [Gilliland et al. \(2013\)](#), H13: [Huber et al. \(2013\)](#), HL14: [Hadden & Lithwick \(2014\)](#), HL16: [Hadden & Lithwick \(2016\)](#), Ha11: [Hartman et al. \(2011\)](#), Ha13: [Harpsoe et al. \(2013\)](#), JH14: [Jontof-Hutter et al. \(2014\)](#), JH15a: [Jontof-Hutter et al. \(2015\)](#), JH15b: [Jontof-Hutter et al. \(2016\)](#), K14: [Kipping et al. \(2014\)](#), L13: [Lissauer et al. \(2013\)](#), Mac14: [Maciejewski et al. \(2014\)](#), Mar14: [Marcy et al. \(2014\)](#), Mas13: [Masuda et al. \(2013\)](#), Mas14: [Masuda \(2014\)](#), Mot15: [Motalebi et al. \(2015\)](#), Mou14: [Moutou et al. \(2014\)](#), N13: [Nesvorný et al. \(2013\)](#), O14: [Ofir et al. \(2014\)](#), Pep13: [Pepe et al. \(2013\)](#), Pet15: [Petigura et al. \(2016\)](#), S14: [Schmitt et al. \(2014\)](#), SO12: [Sanchis-Ojeda et al. \(2012\)](#), V15: [Vanderburg et al. \(2015\)](#), VG14: [Van Grootel et al. \(2014\)](#), W13: [Weiss et al. \(2013\)](#), W16: [Weiss et al. \(2016\)](#), X13: [Xie \(2013\)](#), X14: [Xie \(2014\)](#).

^b The ‘R’ and ‘T’ superscripts indicate RV- and TTV-estimated mass, respectively.